RSC Advances

PAPER

View Article Online
View Journal | View Issue

Cite this: *RSC Adv.*, 2023, **13**, 26925

Synthesis of lenvatinib-loaded upconversion@polydopamine nanocomposites for upconversion luminescence imaging-guided chemo-photothermal synergistic therapy of anaplastic thyroid cancer†

Jingjing Zhou,‡[a] Lina Ma,‡[bc] Zhenshengnan Li,[a] Bowen Chen,[a] Yue Wu[a] and Xianying Meng*[a]

Anaplastic thyroid cancer (ATC) is the most malignant and aggressive of all classifications of thyroid cancer. ATC normally has poor prognosis after classic treatments such as surgery, endocrine therapy, radiotherapy and chemotherapy. Herein, a novel nanocomposite (named as UCNP@PDA@LEN) has been synthesized for chemo-photothermal therapy of ATC, which is based on a $NaErF_4$:Tm^{3+}@$NaYbF_4$@$NaYF_4$:Nd^{3+} upconverting nanoparticle (UCNP) as the core, a near-infrared light (NIR)-absorbing polydopamine (PDA) as the shell, and lenvatinib (LEN) as a chemotherapeutic drug. The as-prepared multifunctional UCNP@PDA@LEN exhibits excellent photothermal conversion capability ($\eta = 30.7\%$), good photothermal stability and reasonable biocompatibility. Owing to the high UCL emission and good tumor accumulation ability, the UCL imaging of mouse-bearing ATC (*i.e.*, C643 tumor) has been achieved by UCNP@PDA@LEN. Under 808 nm NIR laser irradiation, the UCNP@PDA@LEN shows a synergistic interaction between photothermal therapy (PTT) and chemotherapy (CT), resulting in strongly suppressed mouse-bearing C643 tumor. The results provide an explicit approach for developing theranostics with high anti-ATC efficiency.

Received 31st March 2023
Accepted 31st August 2023

DOI: 10.1039/d3ra02121a

rsc.li/rsc-advances

1. Introduction

Thyroid cancer is the most common malignant tumor of the endocrine system.[1,2] The incidence of thyroid cancer has rapidly increased in recent years.[3–6] According to pathological classification, thyroid cancer can be divided into papillary thyroid cancer (PTC), follicular thyroid cancer (FTC), medullary thyroid cancer (MTC) and anaplastic thyroid cancer (ATC).[7–9] ATC is the most malignant pathological type because of its aggressive behavior and resistance to traditional treatments.[10–12] In particular, the one-year survival rate of ATC is very poor, which is less than 20%.[13] The standard treatments of thyroid cancer include surgery, endocrine therapy, radioactive ^{131}I therapy and chemotherapy.[14,15] However, there are certainly side-effects in these methods, for instance, improper operations can cause peripheral nerve injury,[16] long-term use of thyroxine drugs after surgery has negative impacts on the life quality of patients,[17] radiation from radioactive ^{131}I therapy causes damage to the body,[18] and chemotherapy drugs such as sorafenib and lenvatinib (LEN) can lead to the decline of body immunity because of the use of large doses of drugs.[19,20] Most patients of ATC have tumor metastasis to peripheral tissue, organ infiltration and distant organs, when they are diagnosed.[21,22] It is highly desired to develop synergistic therapy of ATC because monotherapy cannot achieve the ideal therapeutic effects.

As a non-invasive method, photothermal therapy (PTT) has several advantages including good controllability and low side effect.[23–25] Due to tissue penetration capacity of light, the PTT may achieve better therapeutic effects on superficial tumors including thyroid cancer than those on deep tissue tumors.[26] Various inorganic nanoparticles (NPs) and organic materials have been used as PTT agents for treatment of tumors.[27–31] Among of them, polydopamine (PDA), a synthetic melanin, has attracted extensive attention since PDA exhibits strong absorption in near-infrared (NIR) region, high photothermal conversion efficiency, excellent biocompatibility and good biodegradability.[32] In addition, PDA is an efficient carrier for loading chemotherapy drugs since it contains abundant

[a]*Thyroid Surgery Department, General Surgery Center, First Hosipital of Jilin University, Changchun, 130021, P. R. China. E-mail: mengxiany@jlu.edu.cn*
[b]*College of Traditional Chinese Medicine, Jilin Agricultural Science and Technology College, Jilin, 132101, P. R. China*
[c]*State Key Laboratory of Electroanalytical Chemistry, Changchun Institute of Applied Chemistry, Chinese Academy of Sciences, Changchun, 130022, P. R. China*

† Electronic supplementary information (ESI) available. See DOI: https://doi.org/10.1039/d3ra02121a

‡ These authors contributed equally to this work.

catechol groups which can form strong π–π stacking with many aromatic drugs.[33–35] It is demonstrated that the synergistic interaction between PTT and chemical therapy (CT) can enhance significantly the outcome of tumor treatment.

Compared with traditional downconversion fluorescent probes, the lanthanide-doped upconversion nanoparticles (UCNPs) have prominent advantages including high optical stability, low autofluorescence background and deep-tissue excitability under NIR excitation, *etc*.[36,37] During last two decades, UCNPs have been extensively used in various bioanalytical and biomedical fields, such as biosensor fabrication, *in vivo* bioimaging, upconversion luminescence (UCL) imaging-guided tumor therapy, *etc.*[38,39] Recently, PDA coated UCNPs (named as UCNP@PDA) have attracted wide interest for fabrication of multifunctional nanoplatforms because UCNP@PDA combine the advantages of PDA and UCNPs.[40–42] For instance, Liu *et al.* constructed a multifunctional nanotheranostic that gathers five functions through the loading doxorubicin (DOX) on UCNP@PDA.[41] Under 808 nm NIR laser irradiation, the as-prepared nanotheranostic shows great synergistic interaction between PTT and CT, resulting in complete suppression of mouse-bearing SW620 tumor without regrowth.

As a multi-target tyrosine kinase inhibitor, lenvatinib (LEN) has clinically approved for the treatment of refractory thyroid cancer.[43–45] LEN can not only target various vascular endothelial growth factor receptors including VEGFR1, VEGFR2 and VEGFR3, but also inhibit other tyrosine kinases involved in pathological angiogenesis, tumor growth and cancer progression.[46] Although the clinical effect of LEN on ATC is remarkable, LEN usually leads to serious adverse effects such as hematopenia, decreased immunity, diarrhea, hair loss and skin toxicity during ATC treatment because of large dosage and non-target accumulation of LEN.[47,48] In recent years, the preparation of nanocarriers for delivering chemotherapy drugs has attracted widespread research. Delivery of chemotherapy drugs *in vivo* through nanocarriers can not only improve the efficacy of chemotherapy drugs, but also reduce the toxic side effects of chemotherapy.[49–52] Therefore, it is essential to explore a new type of nanocarrier to load LEN and achieve targeted drug release in tumor tissue.

Herein, we fabricated a multifunctional nanocomposite (named as UCNP@PDA@LEN) for UCL imaging-guided PTT-CT of ATC through loading LEN on PDA coated $NaErF_4$:Tm^{3+}@$NaYbF_4$@$NaYF_4$:Nd^{3+} UCNP. Owing to its unique properties including strong UCL emission, good photothermal conversion efficiency, and low biotoxicity, excellent UCL imaging capacity and synergistic therapeutic efficacy of UCNP@PDA@LEN is demonstrated in both of *in vitro* cell culture and *in vivo* animal experiments.

2. Experimental section

2.1 Synthesis of UCNP@PDA@LEN

The UCNP and UCNP@PDA were prepared by our previously reported method with slight modification.[41] To synthesis UCNP@PDA, 0.65 mL Igepal CO-520 were added into 10 mL cyclohexane containing 10 mg UCNP. After stirred for 20 min, 75 μL of ammonium hydroxide solution were added into the mixture. The mixture was stirred for 10 min, treated by ultrasonic concussion for 20 min, and stirred for another 30 min, respectively. Subsequently, 50 μL PDA hydrochloride aqueous solution (25 wt%) were injected into the above reaction mixture at a rate of 3 μL min^{-1} and stirred for 24 h. The NPs were precipitated by adding 10 mL ethanol, collected by centrifugation (10 000 rpm, 10 min), and washed with 10 mL ethanol with centrifugation (10 000 rpm, 10 min, 3 times). Finally, the as-obtained UCNP@PDA were redispersed in water and dried by vacuum evaporation.

For loading LEN, 10 mg LEN powder were dissolved in 500 μL DMSO and followed by ultrasonic treatment for 5 min. 6 mg UCNP@PDA were then dispersed in 4 mL 10 × TB (Tris–HCL buffer, pH 7.4), and mixed with 300 μL LEN solution (20 mg mL^{-1} in DMSO). After stirred in the dark for 12 h, the solution was purified by centrifugation (10 000 rpm, 10 min, 3 times). Finally, the as-obtained UCNP@PDA@LEN were redispersed in 300 μL PBS (pH = 7.4), and stored at 4 °C. The loading weight of LEN (W) onto the UCNP@PDA is calculated by the following equation, $W = W_{\text{original LEN}} - W_{\text{LEN in supernatant}}$. Here, $W_{\text{original LEN}}$ is weight of LEN in initial solution, and the $W_{\text{LEN in supernatant}}$ is weight of LEN in the supernatant. The concentration of LEN was determined by the absorbance at the wavelength of 255 nm.

2.2 Measurement of photothermal performance

A series of 1 mL UCNP@PDA solution with different concentrations (0, 0.1, 0.5, 1, 3, and 5 mg L^{-1}) were irradiated by an 808 nm NIR laser with a power density of 1.8 W cm^{-2} for 10 min, respectively. 1 mL UCNP@PDA solution (5 mg L^{-1}) were irradiated with 808 nm laser with various power densities (0, 1.1, 1.5 and 1.8 W cm^{-2}), respectively. During heating-cooling experiment, 1 mL UCNP@PDA solution (5 mg L^{-1}) were exposed to an 808 nm laser with a power density of 1.8 W cm^{-2} for 600 s. Then, the laser was turned off, and the solution was cooled down naturally. The photostability of UCNP@PDA was measured by cycle irradiation. The heating and cooling cycle was repeated 4 times. The temperature changes of solutions were recorded every 20 s by an infrared thermal camera.

2.3 *In vitro* bioimaging

The C643 cells were seeded in 24-well plate (10^4 cells per well) with 500 μL fresh RMPI-1640 culture medium containing 10% FBS and 100 U mL^{-1} penicillin-streptomycin under a humidified 5% CO_2 at 37 °C for 24 h. After washed with 500 μL PBS (3 times), the C643 cells were incubated with 500 μL fresh RMPI-1640 culture medium containing various concentrations (0, 0.1, 0.5, 1, 3 and 5 mg mL^{-1}) of UCNP@PDA and UCNP@PDA@LEN, respectively. After incubated for a period time (2, 4, 6, 8 and/or 12 h), the C643 cells were washed with 500 μL PBS (3 times). The UCL imaging of C643 cells were performed by the fluorescent microscope (Nikon Co., Japan) with a 980 nm NIR-laser irradiation.

2.4 Cell viability measurements

The C643 cells (10^4 cells per well) were seeded in 96-well plate with 100 μL fresh RMPI-1640 culture medium containing 10%

FBS and 100 U mL^{-1} penicillin-streptomycin under a humidified 5% CO_2 at 37 °C for 24 h. After washed with 100 μL PBS (3 times), fresh RMPI-1640 culture medium (100 μL) with various concentrations (0, 0.1, 0.5, 1, 3 and 5 mg mL^{-1}) of LEN, UCNP@PDA and UCNP@PDA@LEN were added, and incubated at same conditions for another 24 h, respectively. To evaluate the photothermal cytotoxicity, normal cultured cells, and LEN, UCNP@PDA and UCNP@PDA@LEN stained cells were irradiated by an 808 nm NIR-laser (1.8 W cm^{-2}) for 10 min, washed with 100 μL fresh PBS (3 times) and cultured with fresh RMPI-1640 culture medium (100 μL) for another 24 h, respectively. Subsequently, the cells were washed with 100 μL fresh RMPI-1640 culture medium (3 times) and 100 μL PBS (3 times), respectively. 100 μL fresh RMPI-1640 culture medium containing 10% MTT reagent were added into per well and incubated for 4 h. Subsequently, the culture medium were removed, and 100 μL DMSO were added into each well. After gently shaking for 10 min, the optical absorption at 490 nm was measured on a Power Wave XS 2 Microplate Spectrophotometer (Purkinje General Co., Beijing, China). The normal cultured C643 cells were employed as control samples. The cell viability was calculated as $(OD_{Sample} - OD_{Blank})/(OD_{Negative\ control} - OD_{Blank}) \times 100\%$. The temperature changes of cells were monitored by the thermal imager. For calcein acetoxymethyl ester (Calcein AM)/propidium iodide (PI) staining experiments, the untreated C643 cells and treated C643 cells were co-stained with 100 μL calcein acetoxymethyl ester (Calcein AM, 1 mg mL^{-1})/propidium iodide (PI, 1 mg mL^{-1}) for 15 min, respectively. The living cells (green) and dead cells (red) were observed by the fluorescence microscope.

2.5 *In vivo* therapy measurement

The animal procedures were in agreement with the guidelines of the Regional Ethics Committee for Animal Experiments established by Jilin University Institutional Animal Care and Use, and approved by the Animal Ethics Committee of Jilin University. To construct subcutaneous tumor model in mice, 1×10^7 C643 cells were suspended in 100 μL RPMI-1640 medium with 50% metragel, and inoculated subcutaneously in female NOD-SCID mice. When the tumor size reached to about 3–4 mm in diameter, the C643 tumor-bearing mice were randomly divided into six groups ($n = 3$), and treated by 100 μL PBS only (Group I), 100 μL PBS plus irradiated by 808 nm NIR-laser (1.8 W cm^{-2}) for 10 min (Group II), 100 μL UCNP@PDA (5 mg mL^{-1}) (Group III), 100 μL UCNP@PDA (5 mg mL^{-1}) plus irradiated by 808 nm NIR-laser (1.8 W cm^{-2}) for 10 min (Group IV), 100 μL UCNP@PDA@LEN (5 mg mL^{-1}) (Group V), and 100 μL UCNP@PDA@LEN (5 mg mL^{-1}) plus irradiated by 808 nm NIR-laser (1.8 W cm^{-2}) for 10 min (Group VI), respectively. The body weights of C643 tumor-bearing mice were recorded every the other day for 14 days, as well as the tumor volumes were measured by a caliper. The tumor volume was calculated by the formula: tumor volume = (tumor length) × (tumor width)^2/2. The PBS, UCNP@PDA and UCNP@PDA@LEN were injected intravenously into C643 tumor-bearing mice through tail vein, respectively. The *in vivo* UCL imaging was performed at predetermined time intervals (0, 4, 8, 12, 24 and 48 h) of post-injection on a home-made *in vivo* imaging system equipped with a 980 nm laser (2.5 W cm^{-2}).[53] The mice were irradiated with an 808 nm laser at 8 h post-injection, and the temperature increases at tumor sites were recorded by thermal imager.

3. Results and discussion

3.1 Synthesis and characterization of UCNP@PDA@LEN

The synthesis procedure of UCNP@PDA@LEN is illustrated in Scheme 1. The $NaErF_4$:Tm^{3+}@$NaYbF_4$@$NaYF_4$:Nd^{3+} UCNP was firstly synthesized by the previously reported strategy.[41] The UCNP@PDA were obtained by reaction of dopamine hydrochloride with hydrophobic $NaErF_4$:Tm^{3+}@$NaYbF_4$@$NaYF_4$:Nd^{3+} UCNPs in the water-in-oil microemulsion.[54,55] The UCNP@PDA@LEN were prepared by directly loading CT drug, LEN on the UCNP@PDA.

The TEM micrographs show that the average sizes of as-prepared UCNP, UCNP@PDA and UCNP@PDA@LEN are 32.0 ± 2.5 nm, 39.0 ± 3.4 nm, and 39.0 ± 3.8 nm, respectively (as shown in Fig. 1). The result indicates that the UCNP@PDA has about 4 nm thickness of PDA layer on UCNP, and loading LEN exhibits negligible effect on the size of UCNP@PDA. The XPS spectra was measured of UCNP, UCNP@PDA and UCNP@PDA, respectively (as shown in Fig. 1). Under 980 NIR excitation, the UCNP shows two emission bands at 546 nm and 660 nm. The UCL emission of UCNP@PDA decreased after coated with PDA shell because PDA is a strong light absorbing material (as shown in Fig. S1†). It further proved that the PDA shell was successfully coated on the surface of UCNP. The characteristic absorption bands of LEN (255 nm and 297 nm) can be clearly seen in the UV-visible spectrum of UNCP@PDA@LEN (as shown in Fig. S2†), indicating the successful loading of LEN on UNCP@PDA. The loading efficiency of LEN is calculated to be 85.7%. The high loading efficiency is mainly due to the π–π stacking and hydrogen bonding between the PDA shell and LEN.

3.2 Photothermal performance of UCNP@PDA

To evaluate its photothermal conversion capability, the various concentrations of UCNP@PDA were irradiated by the 808 nm NIR-laser (1.8 W cm^{-2}), and the solution temperatures were recorded by the infrared thermal camera. As shown in Fig. 2a and b, the temperature of UCNP@PDA solution was increased with the increasing concentration and the power density of 808 nm NIR laser. The photothermal conversion efficiency of UCNP@PDA is calculated to be 30.7%, which is better than previously reported photothermal conversion agents such as Au nanorods and CuS nanoparticles.[56,57] As shown in Fig. 2c, the rapid heating and cooling pattern demonstrates significant photothermal conversion stability and reproducibility of UCNP@PDA. After laser ON/OFF cycles, there was no significant difference in solution temperature change. And there is no obvious absorption change of UCNP@PDA after irradiation for 60 min (as shown in Fig. S3†). The experimental results demonstrate that UCNP@PDA has excellent photothermal

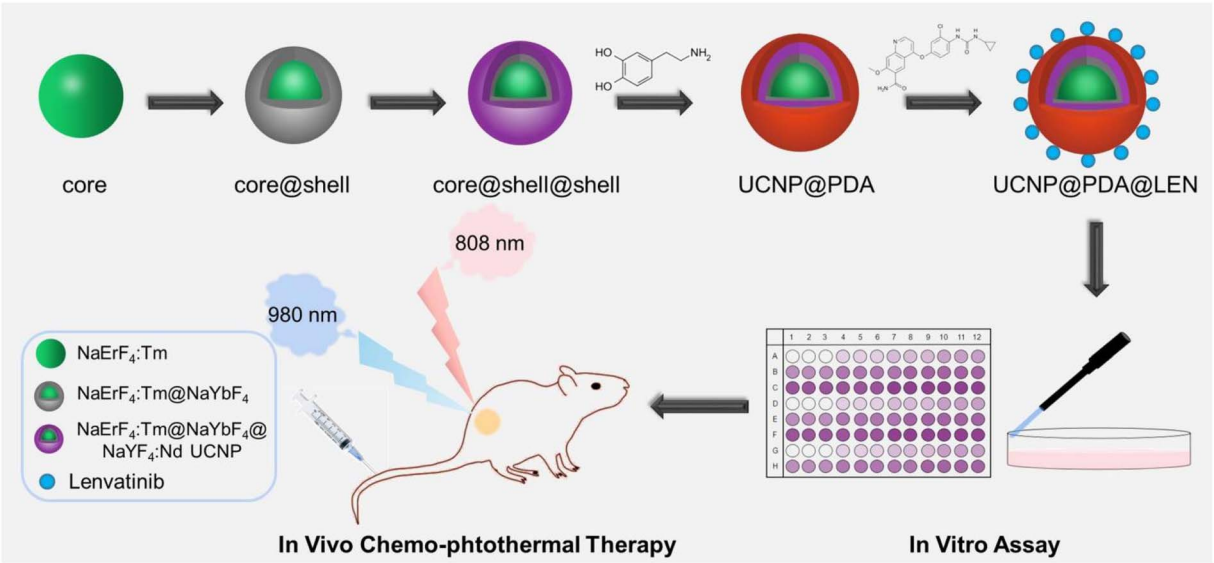

Scheme 1 Schematic illustration of the synthetic process of UCNP@PDA@LEN NPs and application for UCL imaging-guided chemo-photothermal synergistic therapy.

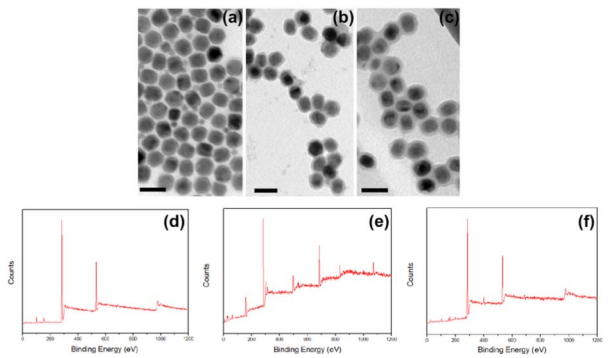

Fig. 1 TEM micrographs of (a) UCNP, (b) UCNP@PDA and (c) UCNP@PDA@LEN, respectively. Scale bar: 50 nm. XPS spectra of (d) UCNP, (e) UCNP@PDA and (f) UCNP@PDA@LEN.

stability. Take the advantages of good photothermal conversion capability and photothermal stability, UCNP@PDA has potential in biomedical and clinical applications as an efficient PTT agent.

3.3 Releasing behaviors of UCNP@PDA@LEN

The releasing behaviors of UCNP@PDA@LEN with or without NIR-laser were investigated at pH 5.0. The release efficiency of LEN is about 22% after 24 h (as shown in Fig. S4†). The slow releasing of LEN is beneficial to the long-term treatment for ATC without requirement of frequent administration. After irradiated by 808 nm NIR-laser (1.8 W cm^{-2}) for 10 min, a burst release of LEN was observed from the UCNP@PDA@LEN. After 808 nm NIR-laser irradiation (3 times), the releasing efficiency reached to 34% after 24 h, which is significantly higher than that without irradiation. The result indicates that 808 nm NIR-laser can effectively stimulate the releasing of LEN, and enhance the anti-tumor effect of UCNP@PDA@LEN. The NIR-responsive release could be used to adjust intracellular amount of free LEN, resulting in reduction of side effects caused by LEN treatment.

3.4 *In vitro* assay

After co-cultured with UCNP@PDA and/or UCNP@PDA@LEN, the C643 cells exhibit strong UCL emission, which are gradually increased with the increasing concentrations of UCNP@PDA@LEN and incubation time (as shown in Fig. 3a, S5 and S6†). The result indicates that UCNP@PDA and UCNP@PDA@LEN can be efficiently uptaken by C643 cells, and exhibit concentration- and time-dependent cellular internalization behavior.

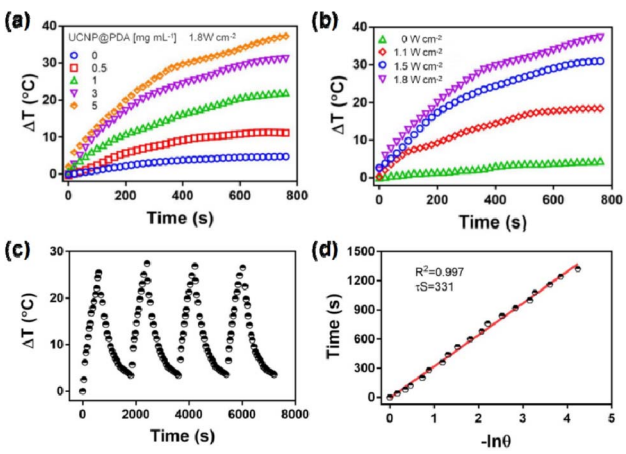

Fig. 2 (a) The solution temperature curves of different concentrations (0, 0.1, 0.5, 1, 3 and 5 mg mL^{-1}) of UCNP@PDA under 1.8 W cm^{-2} 808 nm NIR-laser irradiation. (b) The solution temperature curves of UCNP@PDA (5 mg mL^{-1}) under different laser densities (0, 1.1, 1.5 and 1.8 W cm^{-2}). (c) Heating and cooling curves of UCNP@PDA (5 mg mL^{-1}) irradiated by an 808 nm NIR-laser (1.8 W cm^{-2}) over four ON/OFF cycles. (d) Linear time data *versus* negative natural logarithm of the temperature driving force.

After irradiated by 808 nm NIR-laser (1.8 W cm^{-2}) for 10 min, the temperature of C643 cells are increased with the increasing concentrations of UCNP@PDA and UCNP@PDA@LEN (as shown in Fig. S7†). The temperature can reach to 55 °C when UCNP@PDA@LEN (5 mg mL^{-1}) stained C643 cells were irradiated by 1.8 W cm^{-2} 808 nm NIR laser for 10 min. The cancer cells can be killed efficiently when temperatures is over 50 °C for 4–6 min.[58]

The anticancer ability of UCNP@PDA@LEN was further evaluated by MTT assay (as shown in Fig. 3b). In the absence of NPs, the cells show negligible change of viability with or without NIR-laser irradiation. The viability of C643 cells is still more than 90% when the cells co-cultured with as high as 5 mg mL^{-1} UCNP@PDA, indicating the low cytotoxicity of UCNP@PDA. The cell viabilities are significantly decreased from 83% to 32% with the increasing concentrations of UCNP@PDA@LEN from 0.1 to 5 mg mL^{-1}, indicating a concentration-dependent cytotoxic effect. The result confirms that UCNP@PDA@LEN can effectively lead to apoptosis and necrosis of C643 cells by releasing LEN. After irradiation by 808 nm NIR-laser (1.8 W cm^{-2}) for 10 min, the cell viabilities are dramatically decreased with the increasing concentrations of UCNP@PDA and UCNP@PDA@LEN. In particular, the UCNP@PDA@LEN stained C643 cell viability was decreased to 13%, which is lower than that of UCNP@PDA (38%), suggesting the chemo-photothermal synergistic effect. Due to slowly releasing behavior of LEN from UCNP@PDA@LEN, under same concentration, the LEN loaded on UCNP@PDA@LEN exhibited lower cytotoxicity than that of free LEN. This phenomenon may help to reduce the side effect of LEN. The result is further proved by Calcein AM and PI co-staining assay. The calcein AM and PI fluorescent dyes are used to identify living cells (green) and dead cells (red), respectively. The UCNP@PDA@LEN stained C643 cells exhibited strong PI fluorescence signals after irradiation by 808 nm NIR-laser (as shown in Fig. 3c), which is consistent with the result of MTT assay.

The side effects of the nanocomposites was further evaluated by MTT assay. The normal thyroid cells were cultured with UCNP, UCNP@PDA, UCNP@PDA@LEN for 8 hours, respectively. As shown in Fig. S13,† the viability of normal thyroid cells show negligible change when the cells co-cultured with the nanocomposite, indicating that the nanocomposites have negligible side effects and excellent biological safety.

3.5 *In vivo* assay

The UCL images of the tumor sites were recorded at different time points (0, 4, 8, 12, 24 and 48 h) of post-treatment under 980 nm NIR-laser irradiation. The strongest UCL signal was

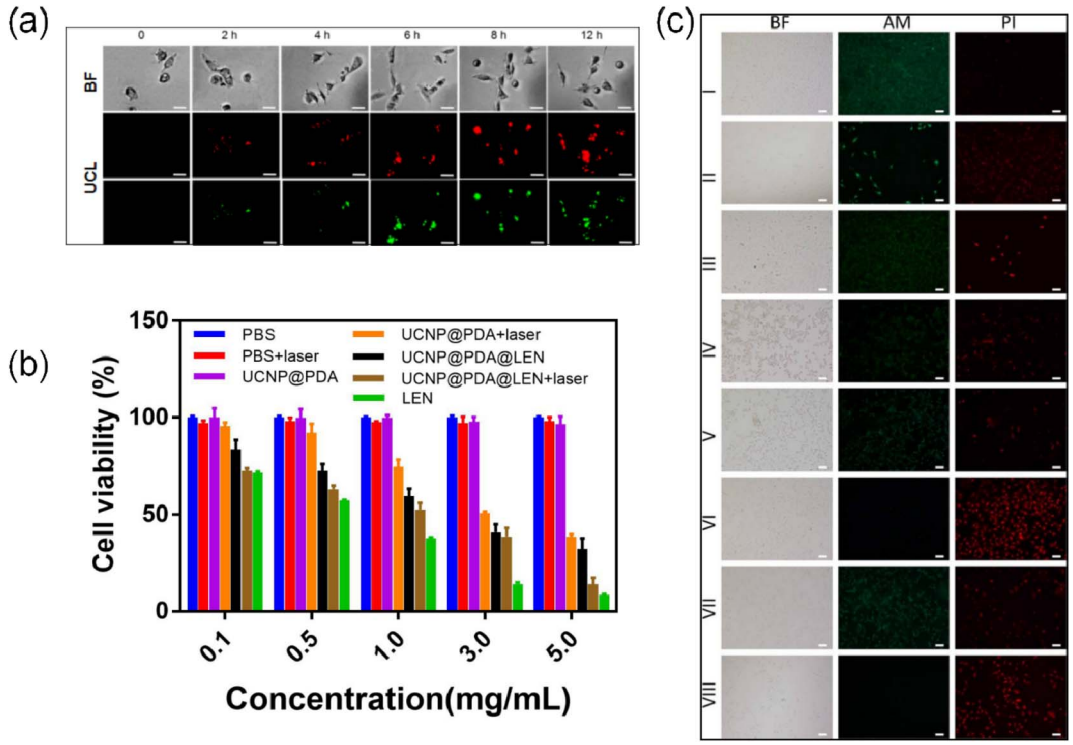

Fig. 3 (a) The bright field (BF) and UCL images of UCNP@PDA@LEN stained C643 cells at different time points. All of scale bars are 20 μm. (b) The cell viabilities of C643 cells after co-cultured with PBS and various concentrations of UCNP@PDA and UCNP@PDA@LEN with or without 808 nm NIR-laser irradiation (1.8 W cm^{-2}, 10 min). The concentrations of LEN are as same as the concentrations of LEN loaded on the correspondent UCNP@PDA@LEN. The error bars mean standard deviations ($n = 5$). (c) BF, Calcein AM and PI fluorescence images of C643 cells after different treatments. The normally cultured C643 cells were used as the control (Group I) and (Group V, 808 nm NIR-laser irradiation for 10 min). The C643 cells were co-cultured with LEN (Group II), UCNP@PDA (Group III), UCNP@PDA@LEN (Group IV), LEN plus 808 nm NIR-laser irradiation for 10 min (Group VI), UCNP@PDA plus 808 nm NIR-laser irradiation for 10 min (Group VII) and UCNP@PDA@LEN plus 808 nm NIR-laser irradiation for 10 min (Group VIII), respectively. All of scale bars are 50 μm.

obtained at 8 h post-injection (As shown in Fig. 4a and S8†). The UCL signal was gradually decreased after 24 h. The result illustrated that the UCNP@PDA@LEN can efficiently accumulate in tumor site, and the accumulation amount of UCNP@PDA@LEN in the tumor site reaches the maximum at 8 h post-injection.

The photothermal effect of UCNP@PDA@LEN was further investigated *in vivo*. The C643 tumor-bearing mice were treated with 100 μL PBS, UCNP@PDA (5 mg mL^{-1}) and UCNP@PDA@LEN (5 mg mL^{-1}) by intravenous injection, respectively. After irradiated by 808 nm NIR-laser (1.8 W cm^{-2}), the tumor temperature of UCNP@PDA and UCNP@PDA@LEN groups were rapidly increased within 10 min, whereas PBS groups (control) exhibited poor increasing of temperatures at tumor sites. The area of high temperature in tumor site reaches maximum at 8 h post-injection (as shown in Fig. 4b and S10†). The results indicated that UCNP@PDA@LEN could be used as an agent for PTT of tumor.

The chemo-photothermal synergistic therapeutic efficiency of UCNP@PDA@LEN was investigated subsequently *in vivo* (as shown in Fig. 5a and b). There is no statistically significant difference in tumor sizes among Group I, Group II and Group III, suggesting that only irradiation by 808 nm NIR-laser and only administration of UCNP@PDA cannot inhibit tumor growth. Although the effective inhibitions of tumor growth were observed in Group IV and Group V, the tumors still grow up gradually. The strongest inhibition of tumor growth was observed in Group VI, and the growth of tumor was almost completely suppressed over a course of 14 days. The result indicates that the UCNP@PDA@LEN can achieve remarkable chemo-photothermal synergistic treatment effect for ATC.

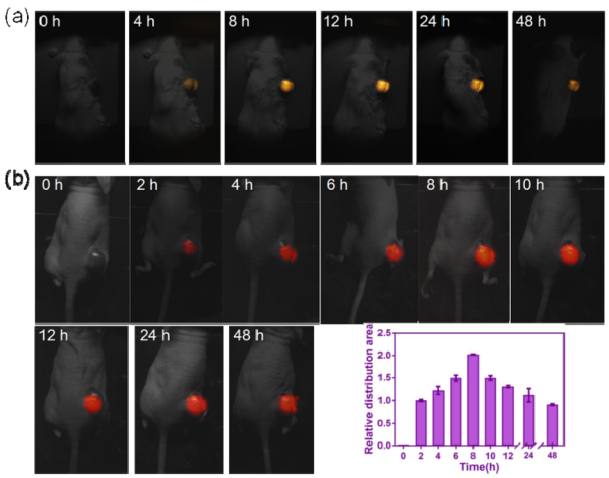

Fig. 4 (a) The UCL images of C643 tumor-bearing mice at different time intervals (0, 4, 8, 12, 24 and 48 h) after injection of UCNP@PDA@LEN. The UCNP@PDA@LEN (5 mg mL^{-1}) were intravenously injected into C643 tumor-bearing mice through tail vein. The tumor sites were irradiated by 980 nm NIR-laser (2.5 W cm^{-2}). (b) The thermal images of C643 tumor-bearing mice at different time intervals (0, 2, 4, 6, 8, 10, 12, 24 and 48 h) after intravenous injection of UCNP@PDA@LEN. The tumor sites were irradiated by 808 nm NIR-laser (1.8 W cm^{-2}) for 10 min. The Histogram represents the corresponding area of high temperature at different time intervals.

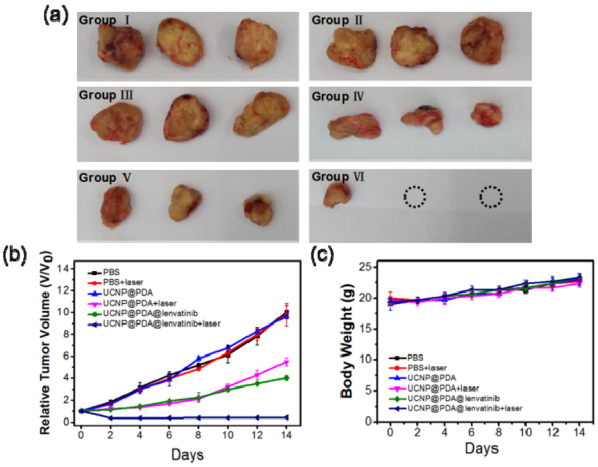

Fig. 5 (a) Photographs of tumors collected from different treatment groups after 14 days. (b) The tumor growth curves and (c) body weight curves of C643 tumor-bearing mice following different treatments.

The body weights of C643 tumor-bearing mice in all experimental groups are no statistical difference during 14 days (as shown in Fig. 5c). In addition, the result of hematology analysis shows that there is nearly no difference in all experimental groups (as shown in Table S1†), which proves that the low toxicity and good biological safety of UCNP@PDA@LEN. The H&E staining result shows that there is no histological injury or inflammation of the main organs after administration, which further proves the good biosafety of UCNP@PDA@LEN (as shown in Fig. S11†). The Y, Nd, Tm and Yb element content in major organs of C643 tumor-bearing mice at 8 h post injection of UCNP@PDA@LEN were measured, as shown in the Fig. S14,† after 8 hours of injection of UCNP@PDA@LEN into C643 tumor-bearing mice, the distribution in the liver and tumor site was the highest.

4. Conclusions

In summary, a multifunctional nanocomposite (UCNP@PDA@LEN) has been developed for UCL imaging-guided chemo-photothermal synergistic therapy of ATC through loading TC drug LEN on the PDA coated UCNP (UCNP@PDA). The as-prepared UCNP@PDA@LEN has several advantages including strong photothermal conversion efficiency and good biosafety. Results of both *in vitro* experiments and *in vivo* experiments demonstrate that UCNP@PDA@LEN exhibit a high anti-tumor capacity owing to the synergistic PTT and CT effect under the 808 nm NIR-laser irradiation. In addition, the UCNP@PDA@LEN can be used as a probe for UCL imaging. This research provides a new possibility for the clinical treatment of ATC.

Author contributions

Jingjing, Zhou: performing the experiments and original draft writing. Lina Ma: design of methodology, visualization/data presentation, editing the draft and funding acquisition. Zhenshengnan, Li: helped with data analysis. Bowen Chen: prepared

for all the regents and materials. Yue Wu: data collection. Xianying Meng: formulation of overarching research goals and aims, oversight and leadership responsibility for the research activity planning and execution and funding acquisition.

Conflicts of interest

There are no conflicts to declare.

Acknowledgements

The author would like to thank the National Natural Science Foundation of China (Grant no. 62001449), Jilin Provincial Science and Technology Department (Grant no. 20210204049YY and no. 20200201357JC) and Beijing Cihua Medical Development Foundation (J2022107012) for financial support.

References

1 T. Yu, L. Tong, Y. Ao, G. Zhang, Y. Liu and H. Zhang, *J. Photochem. Photobiol., B*, 2019, **197**, 111534.
2 J. H. D. Bassett and G. R. Williams, *Endocr. Rev.*, 2016, **37**, 135–187.
3 B. R. Roman, L. G. Morris and L. Davies, *Curr. Opin. Endocrinol. Diabetes Obes.*, 2017, **24**, 332–336.
4 M. Colonna, Z. Uhry, A. V. Guizard, P. Delafosse, C. Schvartz, A. Belot and P. Grosclaude, *Cancer Epidemiol.*, 2015, **39**, 511–518.
5 J. D. Cramer, B. Burtness, Q. T. Le and R. L. Ferris, *Nat. Rev. Clin. Oncol.*, 2019, **16**, 669–683.
6 H. Sung, J. Ferlay, R. L. Siegel, M. Laversanne, I. Soerjomataram, A. Jemal and F. Bray, *Ca-Cancer J. Clin.*, 2021, **71**, 209–249.
7 S. L. Asa, *Endocrinol. Metab. Clin. North Am.*, 2019, **48**, 1–22.
8 A. Prete, P. Borges de Souza, S. Censi, M. Muzza, N. Nucci and M. Sponziello, *Front. Endocrinol.*, 2020, **11**, 102.
9 M. Gawin, A. Wojakowska, M. Pietrowska, Ł. Marczak, M. Chekan, K. Jelonek, D. Lange, R. Jaksik, A. Gruca and P. Widłak, *Mol. Cell. Endocrinol.*, 2018, **472**, 68–79.
10 E. Molinaro, C. Romei, A. Biagini, E. Sabini, L. Agate, S. Mazzeo, G. Materazzi, S. Sellari-Franceschini, A. Ribechini, L. Torregrossa, F. Basolo, P. Vitti and R. Elisei, *Nat. Rev. Endocrinol.*, 2017, **13**, 644–660.
11 M. K. Gule, Y. Chen, D. Sano, M. J. Frederick, G. Zhou, M. Zhao, Z. L. Milas, C. E. Galer, Y. C. Henderson, S. A. Jasser, D. L. Schwartz, J. A. Bankson, J. N. Myers and S. Y. Lai, *Clin. Cancer Res.*, 2011, **17**, 2281–2291.
12 M. R. Haymart, *Endocr. Pract.*, 2021, **27**, 1260–1263.
13 M. Zhou, Y. Chen, M. Adachi, X. Wen, B. Erwin, O. Mawlawi, S. Y. Lai and C. Li, *Biomaterials*, 2015, **57**, 41–49.
14 D. F. Schneider and H. Chen, *Ca-Cancer J. Clin.*, 2013, **63**, 373–394.
15 J. Martínez Trufero, J. Capdevilla, J. J. Cruz and D. Isla, *Clin. Transl. Oncol.*, 2011, **13**, 574–579.
16 T. S. Wang and J. A. Sosa, *Nat. Rev. Endocrinol.*, 2018, **14**, 670–683.
17 B. Biondi and D. S. Cooper, *Endocrine*, 2019, **66**, 18–26.
18 S. Izadyar, M. Pashnehsaz, A. Takavar, S. Zakariaee, M. Mahmoudi, R. Paydar and P. Geramifar, *World J. Nucl. Med.*, 2016, **15**, 173.
19 T. Kimura, Y. Kato, Y. Ozawa, K. Kodama, J. Ito, K. Ichikawa, K. Yamada, Y. Hori, K. Tabata, K. Takase, J. Matsui, Y. Funahashi and K. Nomoto, *Cancer Sci.*, 2018, **109**, 3993–4002.
20 J. Wang, R. Liu, Y. Zhao, Z. Ma, Z. Sang, Z. Wen, X. Yang and H. Xie, *Front. Oncol.*, 2021, 11.
21 D. Olfa, L. Sami, S.-F. Céline, L. Jean-Christophe and C. Christian, *BMC Cancer*, 2011, **11**, 469–469.
22 C. Renaud De, B. Eric and B. Anne, *Int. J. Radiat. Oncol., Biol., Phys.*, 2004, **60**, 1137–1143.
23 J. Li, L. Zheng, C. Li, Y. Xiao, J. Liu, S. Wu and B. Zhang, *Biomater. Sci.*, 2021, **9**, 4648–4661.
24 X. Gu, K. Liao, X. Lu, W. Huang and Q. Fan, *Front. Bioeng. Biotechnol.*, 2021, **9**, 780993.
25 H.-X. Tang, C.-G. Liu, J.-T. Zhang, X. Zheng, D.-Y. Yang, R. K. Kankala, S.-B. Wang and A.-Z. Chen, *ACS Appl. Mater. Interfaces*, 2020, **12**, 47289–47298.
26 N. Alifu, L. Yan, H. Zhang, A. Zebibula, Z. Zhu, W. Xi, A. W. Roe, B. Xu, W. Tian and J. Qian, *Dyes Pigm.*, 2017, **143**, 76–85.
27 Q. Cheng, L. Yue, J. Li, C. Gao, Y. Ding, C. Sun, M. Xu, Z. Yuan and R. Wang, *Small*, 2021, **17**, 2101332.
28 Y. Wang, X. Li, P. Chen, Y. Dong, G. Liang and Y. Yu, *Nanoscale*, 2020, **12**, 1886–1893.
29 T. Sun, J.-H. Dou, S. Liu, X. Wang, X. Zheng, Y. Wang, J. Pei and Z. Xie, *ACS Appl. Mater. Interfaces*, 2018, **10**, 7919–7926.
30 J. Li, C. Liu, Y. Hu, C. Ji, S. Li and M. Yin, *Theranostics*, 2020, **10**, 166–178.
31 D. Wang, Z. Zhang, L. Lin, F. Liu and X. Chen, *Biomaterials*, 2019, **223**, 119459.
32 X. Zhang, X. Nan, W. Shi, Y. Sun, H. Su, Y. He, X. Liu, Z. Zhang and D. Ge, *Nanotechnology*, 2017, **28**, 295102.
33 H. Kim, J. Jang, D. Byun, H. S. Kim and W. Choi, *ChemSusChem*, 2019, **12**, 5253–5264.
34 X. Liu, J. Cao, H. Li, J. Li, Q. Jin, K. Ren and J. Ji, *ACS Nano*, 2013, **7**, 9384–9395.
35 V. Ball, D. D. Frari, V. Toniazzo and D. Ruch, *J. Colloid Interface Sci.*, 2012, **386**, 366–372.
36 J. Chen, D. Zhang, Y. Zou, Z. Wang, M. Hao, M. Zheng, X. Xue, X. Pan, Y. Lu, J. Wang and B. Shi, *J. Mater. Chem. B*, 2018, **6**, 7862–7870.
37 A. N. Generalova, B. N. Chichkov and E. V. Khaydukov, *Adv. Colloid Interface Sci.*, 2017, **245**, 1–19.
38 S. Zeng, H. Wang, W. Lu, Z. Yi, L. Rao, H. Liu and J. Hao, *Biomaterials*, 2014, **35**, 2934.
39 P. Nguyen, S. Son and J. Min, *J. Nanosci. Nanotechnol.*, 2014, **14**, 157–174.
40 Y. Cen, W.-J. Deng, Y. Yang, R.-Q. Yu and X. Chu, *Anal. Chem.*, 2017, **89**, 10321–10328.
41 F. Liu, X. He, Z. Lei, L. Liu, J. Zhang, H. You, H. Zhang and Z. Wang, *Adv. Healthcare Mater.*, 2015, **4**, 559–568.
42 Q. Wang, Z. Fang, Y. Wu, M. Zhang and G. Shi, *Analyst*, 2020, **145**, 7191–7196.

43 E. Song, M. Kim, E. Y. Kim, B. H. Kim, D. Y. Shin, H. C. Kang, B. C. Ahn, W. B. Kim, Y. K. Shong, M. J. Jeon and D. J. Lim, *Thyroid*, 2020, **30**, 732–738.
44 M. H. Taylor, S. Takahashi, J. Capdevila, M. Tahara, S. Leboulleux, N. Kiyota, C. E. Dutcus, R. Xie, B. Robinson, S. Sherman, M. A. Habra, R. Elisei and L. J. Wirth, *Thyroid*, 2021, **31**, 1226–1234.
45 A. Berdelou, I. Borget, Y. Godbert, T. Nguyen, M. E. Garcia, C. N. Chougnet, A. Ferru, C. Buffet, O. Chabre, O. Huillard, S. Leboulleux and M. Schlumberger, *Thyroid*, 2018, **28**, 72–78.
46 M. E. Cabanillas and M. A. Habra, *Cancer Treat. Rev.*, 2016, **42**, 47–55.
47 A. Gunaydin Akyildiz, T. Boran, A. T. Jannuzzi and B. Alpertunga, *Toxicol. Appl. Pharmacol.*, 2021, **423**, 115577.
48 Z. Ye, L. Wu, X. Zhang, Y. Hu and L. Zheng, *J. Pharm. Biomed. Anal.*, 2021, **202**, 114161.
49 X. You, L. Wang, J. Zhang, T. Tong, C. Dai, C. Chen and J. Wu, *Chin. Chem. Lett.*, 2023, **34**, 107720.
50 S. Peng, X. Zhang, H. Huang, B. Cheng, Z. Xiong, T. Du, J. Wu and H. Huang, *APL Bioeng.*, 2022, **6**, 046106.
51 H. Hu, Z. Zhang, Y. Fang, L. Chen and J. Wu, *Chin. Chem. Lett.*, 2023, **34**, 107953.
52 Y. Zhu, Y. Wu, S. Li, X. Yuan, J. Shen, S. Luo, Z. Wang, R. Gao, J. Wu and L. Ge, *Chem. Eng. J.*, 2022, **446**, 137321.
53 L. Ma, F. Liu, L. Zhen and Z. Wang, *Biosens. Bioelectron.*, 2017, **87**, 638–645.
54 X. Wang, H. Li, F. Li, X. Han and G. Chen, *Nanoscale*, 2019, **11**, 22079–22088.
55 W. Wang, Z. Feng, B. Li, Y. Chang, X. Li, X. Yan, R. Chen, X. Yu, H. Zhao, G. Lu, X. Kong, J. Qian and X. Liu, *J. Mater. Chem. B*, 2021, **9**, 2899–2908.
56 L. Dong, G. Ji, Y. Liu, X. Xu, P. Lei, K. Du, S. Song, J. Feng and H. Zhang, *Nanoscale*, 2018, **10**, 825–831.
57 D. K. Roper, W. Ahn and M. Hoepfner, *J. Phys. Chem. C*, 2007, **111**, 3636–3641.
58 J. R. Melamed, R. S. Edelstein and E. S. Day, *ACS Nano*, 2015, **9**, 6–11.